Postprint of: Falkowska A., Seweryn A., Fatigue of titanium alloy Ti_6Al_4V with diamond structure obtained by Laser Power Bed Fusion method, INTERNATIONAL JOURNAL OF FATIGUE Vol. 163 (2022), 107079, DOI: 10.1016/j.ijfatigue.2022.107079

Fatigue of titanium alloy Ti6Al4V with diamond structure obtained by Laser Power Bed Fusion method

Anna Falkowska[1], Andrzej Seweryn[2]

[1] Department of Mechanics and Applied Computer Science, Faculty of Mechanical Engineering, Bialystok University of Technology, 45C Wiejska, Bialystok, 15-351, Poland

[2] Faculty of Mechanical Engineering and Ship Technology, Gdansk University of Technology, 11/12 Gabriela Narutowicza, Gdansk, 80-233, Poland

Nomenclature

A_{eff} – effective elongation

c – exponent in dependency (1)

E^{eff} – effective axial modulus of elasticity

N_f – number of cycles until sample failure

$\overline{N_f}$ – average numer of cycles until sample failure

n - constant

p – porosity

R^2 – coefficient of determination

$\Delta\omega$ – increment of the damage state variable

ε^{eff} – effective strain

ν^{eff} – effective Poisson's ratio

σ_a^{eff} – effective stress amplitude

σ_u^{eff} – effective tensile strength

$\sigma_{0.2}^{eff}$ – effective conventional yield point

σ_{max}^{eff} – maximum effective stress in loading cycle

σ^* - normalized stress value

σ_0^{eff} – critical effective stress

ω – effective scalar damage state variable

ABSTRACT

This paper presents the results of fatigue tests conducted on Ti6Al4V titanium alloy with diamond structure obtained by the Laser Power Bed Fusion method. Samples used in tests were printed with porosities: 81%, 73%, 50%, 34% and near-zero porosity. Samples were subjected to cyclic tests with a constant stress amplitude. The number of cycles until sample failure was registered. Obtained fatigue test results made it possible to determine simple, semi-empirical dependencies making it possible to forecast the fatigue life of Ti6Al4V titanium alloy with diamond structure obtained by the Laser Power Bed Fusion method under conditions of uniaxial, cyclically variable loads. The experimental results revealed that the initiation of the macro-crack occurred already with a small number of cycles. This was caused by the presence of two types

of notches: technological micro-notches between particles of melted powder and notches related to the shape of the diamond structure itself. Microscopic observations of the fatigue fractures of samples were carried out, both on those subjected to low-cycle tests and those subjected to high-cycle tests. This made it possible to identify crack initiation and damage accumulation mechanisms as well as to propose numerical dependencies for samples of the tested structure. For this purpose, it is necessary to determine only the tensile strength of the given metamaterial and the fatigue characteristic for the given porosity.

Keywords: titanium alloys, diamond structure, fatigue life, Laser Power Bed Fusion, 3D printing, metamaterials

Introduction

Laser Power Bed Fusion additive manufacturing (AM) methods utilize laser energy and are mainly intended for manufacturing components from metal alloys [1], [2]. This makes it possible to produce components with complex shapes, varied structure or density. Because of this, 3D printing is very popular among modern manufacturing methods and has an influence on many areas of modern life. First of all, it enables the rapid production of widely understood prototypes, without the need for advanced technological processes. However, during production, the applied printing precision may significantly influence the unit price of the finished component [3], [4], [5]. There are many applications for components produced by additive manufacturing methods. From the aviation and automotive industries, through the creation of abrasive materials [6], up to medicine [7]. And it is precisely medicine that is the second field after the automotive industry where components manufactured by additive manufacturing techniques are applied most often. 3D printing methods can be used to produce implants or prostheses, surgical instruments and also anatomical models [5]. Use of these techniques for biomedical applications is characterized by a series of advantages that are not present in the case of components manufactured by conventional methods [8], [9]. Above all, they concern the possibility of obtaining an arbitrary, but at the same time optimal, structure of the appropriate porosity and shape [10], [11], [12]. The application of incremental methods also makes it possible to obtain the appropriate surface quality thanks to laser polishing [13].

Among the metallic biomaterials successfully applied in modern medicine, components based on titanium have gained the greatest popularity. This is possible mainly due to the excellent features, such as biocompatibility, resistance to wear and corrosion [14], [15]. These features have caused titanium alloys to become competitors to other metallic biomaterials, including steel or cobalt-based alloys [16], [17]. Considering

the fact that the structure of bone tissue is non-uniform, the introduction of a component made of solid material to fill in for lost bone is not a good solution, as there are enormous differences in modulus of elasticity values. The stiffness of such a design (implant) can be reduced by introducing a porous component [8], [18], with mechanical properties (particularly stiffness) similar to those of bone tissue [19], [20]. Additionally, a porous implant structure enables faster overgrowth with bone tissue, and hence, better "fixation" of the implant in the human body [21], [22]. One method making it possible to create porous structures is the method where powder is selectively melted by a laser beam, which is an additive manufacturing method [23], [24]. Moreover, components produced by melting powder using a laser guarantee better early osteointegration in comparison to implants manufactured from pure titanium or acid-etched implants [25]. Generally, even polishing of components manufactured by AM methods for biomedical applications is not required, as it impedes overgrowth of the implanted elements with bone tissue [26].

The application of the appropriate values of material and technological parameters conditions the achievement of a uniform structure free of defects, which increases the life of manufactured parts, above all. This is possible thanks to Laser Power Bed Fusion method, which, in contrast to Selective Laser Sintering, uses a higher energy density, enabling full melting of powders. In the case of non-porous structures, it is possible obtain a density similar to theoretical [27]. And it is precisely this, not the treatment process, but the structure of the printed component, that plays a critical role in fatigue tests [28]. Obtaining the proper structure is possible thanks to the application of the appropriate laser power. This is particularly important in components intended for biomedical application [29], [30]. It was demonstrated that, thanks to the LPBF method, it is possible to create a highly porous scaffolding, the mechanical properties of which are very similar to the properties of bone tissue [31], [32], [33]. The paper by Choo et al. [34] presents the microstructure of 316L steel alloys manufactured by the LPBF method using different laser powers and constant scanning speed, captured using a microtomography machine. A linear dependency was demonstrated between increasing porosity and decreasing laser power. Similar observations were made in the work of du Plessis [35], where the porosity of Ti6Al4V titanium alloy's structure was made dependent on laser power. Therefore, based on the results presented, optimal laser power during the 3D printing process can be estimated.

Performing extensive fatigue tests requires pre-determination of the effective strength properties of the analyzed structures. This is possible thanks to tests under monotonic loading conditions, mainly involving

tension or compression of the tested sample. They provide much valuable information, pertaining, among other things, to strength, but also to the stiffness of the tested material or design [36], [37]. In the case of structures created by means of LPBF, one can generally find papers presenting an analysis of the strength of samples with solid filling [37]. There are publications that determine the fatigue life of lattice structures, but often the results refer to a single degree of compaction [38]. In this publication, fatigue tests of structures produced by LPBF method and using hot isostatic pressing method were carried out. There are also publications concerning comparisons of this type of material to classical samples produced from a rod drawn by the turning method [39] or samples printed with consideration of the given structure's shape and orientation [40]. In the case of strength tests of Ti6Al4V titanium alloys of a specific structure, particularly the diamond structure, with various porosities, the paper by Falkowska et al. [41] can be a starting point, as it determined effective values of strength properties in reference to the degree of compaction of the diamond structure. In this work the samples with dimond structures and different porosity were subjected to a monotonic tensile test. This was the beginning of further strength and fatigue analyses. Some information can be a point of reference, especially when comparing studies that have been conducted independently of each other. Some publication present a comparison of the strength properties and fatigue life of lattice structures, including diamond [42], [43], [44]. The work of Van Hoorreweder and Kruth [45] is also noteworthy, in which an analysis of the fatigue life of titanium alloys with diamond structure, with and without chemical surface treatment, is presented. However, the test results refer only to samples with a single porosity.

This paper presents the results of experimental fatigue life tests conducted on Ti6Al4V titanium alloy with diamond structure obtained by the Laser Power Bed Fusion method. Samples with varying compaction of the structure, as well as samples with near-zero porosity, were used in tests. Tests were conducted under uniaxial, cyclically variable loading conditions (symmetrical tension-compression). Microscopic analysis of sample fractures are also presented, based on which crack development and structural fracture mechanisms were identified. The tests performed made it possible to determine the influence of structure compaction on fatigue life as well as to develop a simple model for forecasting the fatigue life of titanium alloys with diamond structure.

1. Test stand and samples

Samples for experimental tests were produced using the Laser Power Bed Fusion (LPBF) method. This method enables the manufacture of designs of any structure and degree of compaction. Samples were produced from LaserForm^{TM}Ti Gr.23 powder. The chemical composition of this powder is given in Table 1. Samples of diamond structure, with various porosities, were used in tests. Samples were designed and produced at Medgal® Orthopeadic Implants & Instruments, which is concerned with the manufacture of medical implants and tools. STL files generated in 3DXpert software for SolidWorks were imported into a ProX DMP 320 printer. This is a very efficient machine that makes it possible to control the technological process and reprocess powder.

Table 1. The chemical composition of the powder used to samples production [46]

LaserForm^{TM}Ti Gr 23 (ASTM E8M)								
Al	C	Fe	H	N	O	V	Y	Others together
5.50-6.50%	≤0.08%	≤0.25%	≤0.12%	≤0.03%	≤0.13%	3.50-4.50%	≤0.005%	≤0.40%

The applied additive manufacturing method of manufacturing the samples enabled the achievement of correct and repeatable structures. This was mainly possible thanks to the application of specific technological parameters of the process. Some of them have been presented in Table 2. Thanks to this 3D printing technique, samples with a diamond structure were produced, with varying degrees of compaction, and hence, varying porosities, on the order of: p=81%, p=73%, p=50% and p=34%, as well as samples with solid filling and of the shape shown in figure 1.

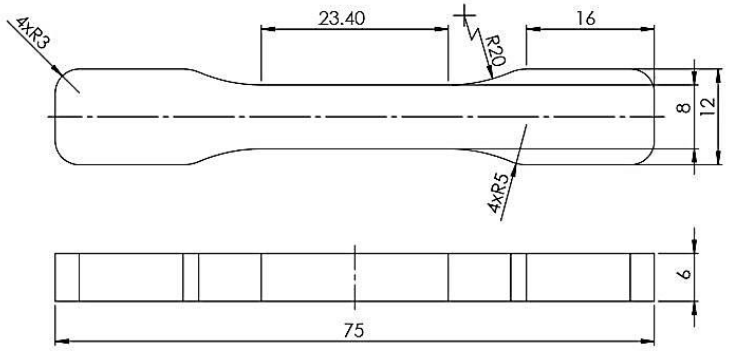

Fig. 1. Dimensions of sample for experimental tests of Ti6Al4V titanium alloys made using the LPBF method

Table 2. Values of technological parameters used in the process of creating samples using the LPBF method

Printer parameter	Value
Scanning speed	400 mm/s
Layer thickness	60 μm
Printing time	35 – 100 min
Laser Power	500 W/Fiber laser
Gas Requirements	Argon

Internal stresses are generated during the technological process of sample production. This is an undesirable effect. In order to remove these stresses, the printed samples were placed in a vacuum furnace at 920°C for five hours. Next, the samples were cut off from the working platform and subjected to finishing treatment, i.e. sanding and polishing. Test-ready samples are shown in figure 2.

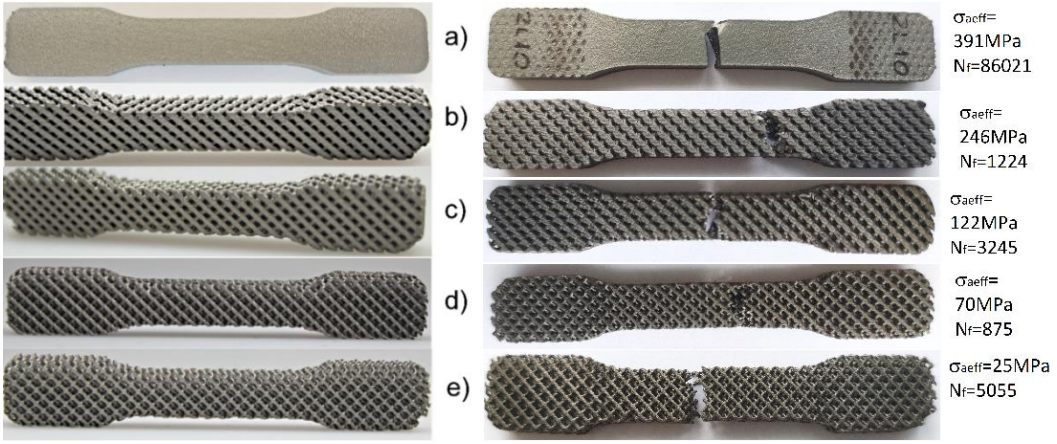

Fig. 2. Samples of Ti6Al4V titanium alloy made by LPBF method, before and after fatigue tests, with porosities: near 0 (a); 34% (b); 50% (c); 73% (d); 81% (e).

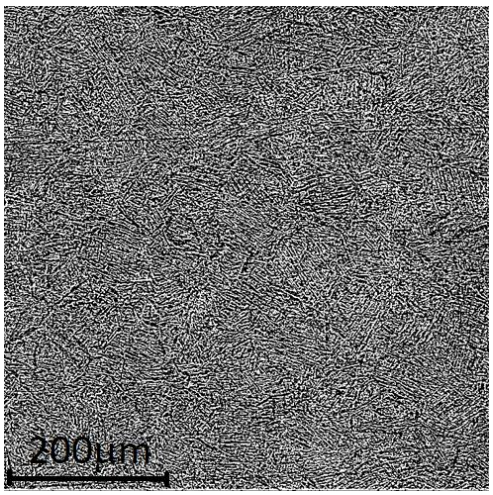

Fig. 3. Microstructure of Ti6Al4V titanium alloy

In addition, a metallographic view of Ti6Al4V titanium alloy (with near-zero porosity) was prepared (fig. 3). A typical structure for this material when obtained by an additive manufacturing method can be observed. Individual grains are defined by clusters of phases oriented parallel to one another: α and β.

Despite the repeatability of the produced structures, it is difficult to obtain a porosity that is precisely as planned. Many factors influence this, for example, the fact that powder grains are not always arranged evenly during melting. This has an effect on the final form of the actual geometry, which differs from the geometry in the CAD model, and thus, may cause reduction of strength properties or fatigue life [47], [48]. This is why the actual porosity of the designed structures was verified gravimetrically and via microtomographic imaging. It can be observed that the porosities of the printed samples differ slightly from the porosity planned at the sample designing stage (Tab 3) [49].

Table 3. Types of samples of Ti6Al4V titanium alloy obtained by the LPBF method used in the tests [49].

Type of sample	Theoretical porosity [%]	Real porosity by CT [%]	Real porosity by microCT [%]
Type 1	81	78.3	78.4
Type 2	73	68.7	69.1
Type 3	50	40.2	45.1
Type 4	34	22.5	28.1

Tensile and fatigue life tests were carried out on a servo-hydraulic MTS 858 Mini Bionix testing machine with Flex Test SE digital control. Strain measurement was realized via an axial Instron 2620-201 extensometer with a measuring base of 25 mm. Samples were placed in special holders of the strength machine (fig. 4). These holders accounted for the shape applied as the grip of the samples as well as for the nature of the tested material, which was characterized by low strength and stiffness and by substantial porosity of structure. Fatigue tests of samples involved their uniaxial tension-compression with a constant stress amplitude and cycle asymmetry factor equal to -1. The defined load levels were estimated based on a prior monotonic tensile test performed on Ti6Al4V titanium alloy samples of varying porosities.

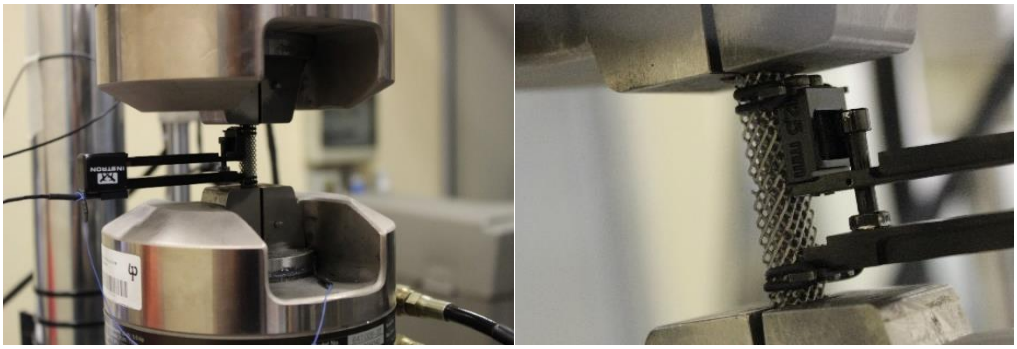

Fig. 4. Sample made of Ti6Al4V titanium sinter with 81% porosity, placed in the testing machine

2. Experimental fatigue life tests of Ti6Al4V titanium alloy with diamond structure and various porosities

2.1. Results of uniaxial tensile tests

Performed monotonic tensile tests made it possible to determine dependencies of effective stress with respect to effective strain (fig. 5) and to distinguish fundamental effective strength properties of structures (Table 4), such as: effective axial modulus of elasticity E^{eff}, effective Poisson's ratio ν^{eff}, effective tensile strength $\sigma_{\text{u}}^{\text{eff}}$, effective conventional yield point $\sigma_{0.2}^{\text{eff}}$ and effective elongation A_{eff} ("effective", meaning in reference to averaged uniform material). Obtained values were made dependent on the structure's degree of compaction. It can be seen that as the density increases, the effective strength properties of the tested structures increase. A fourfold decrease in the porosity of a diamond structure results in an increase in Young's modulus by more than 10 times and in tensile strength by more than 6 times. The value of relative elongation also increases. However, it was not possible to determine the dependence of this value on an increase in the degree of compaction. This was caused by the fact that samples with 34% porosity had lower elongation than samples with 50% porosity. This probably resulted from the technological process itself when creating a diamond structure with a defined degree of compaction. The designing of the structure with lower porosity occurs due to the thickening of the beads. Therefore, a small radius of rounding can be observed, which results in the formation of relatively sharp notches. A detailed analysis of the effects of the technological process of diamond structure samples with different degrees of compaction has been made using computer microtomography and described in Doroszko et al [49]. The stress concentration areas marked in this paper may explain the significant decrease of the effective strain value.

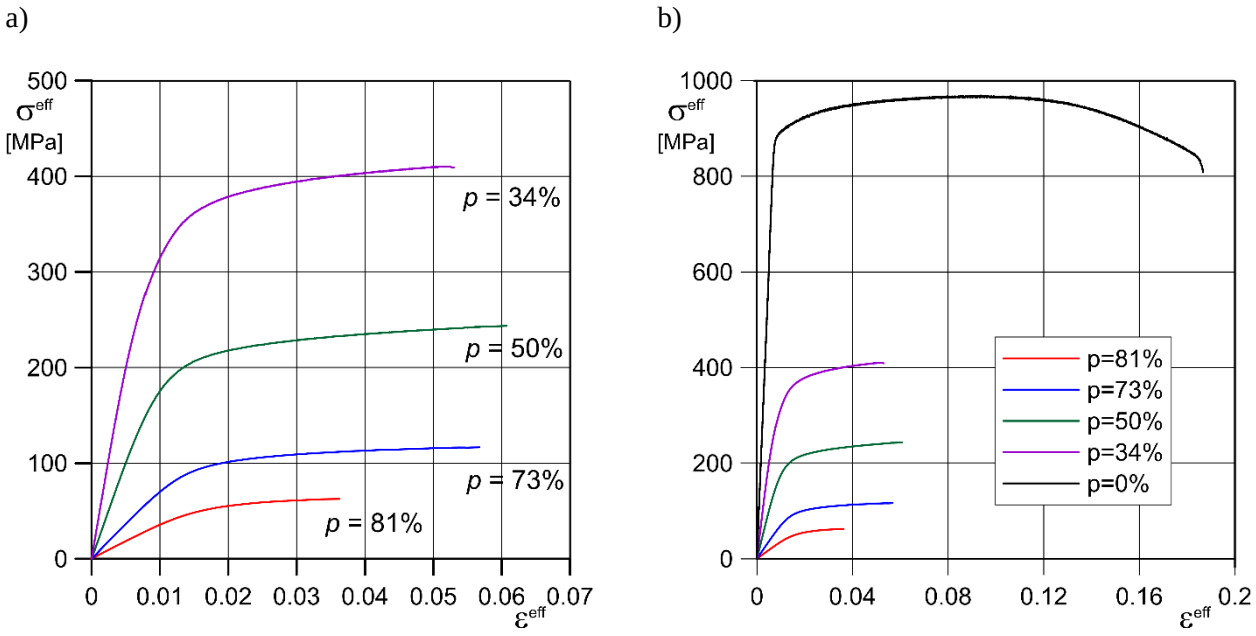

Fig. 5. Averaged monotonic tensile curves of Ti6Al4V titanium alloys with diamond structure and different porosities (a); compared to near-zero porosity samples, obtained by 3D printing [41]

Table 4. Averaged effective strength properties of samples made of Ti6Al4V titanium alloy with different porosities, produced by the LPBF method [41]

p [%]	E^{eff} [GPa]	ν^{eff}	$\sigma_u{}^{eff}$ [MPa]	$\sigma_{0.2}{}^{eff}$ [MPa]	A^{eff} [%]
81	3.7	0.42	62.6	50.3	3.6
73	7.4	0.35	117.2	90.8	6.1
50	20.4	0.32	244.2	193.5	6.4
34	41.8	0.31	410.0	331.7	5.2
0	118.7	0.30	975.1	898.8	18.9

2.2. Results of fatigue life tests

As previously mentioned, the set loading levels were defined based on monotonic tensile tests of samples with specific porosities. The applied effective stress amplitude amounted to, in sequence: $\sigma_a{}^{eff}/\sigma_u{}^{eff}$ = 0.2, 0.3, 0.4, 0.5, 0.6 and 0.7. Moreover, in the case of samples of higher porosity (p = 81%), fatigue tests with the application of higher effective stress amplitude were not possible. This was due to the loss of stability (buckling) of compressed samples prior to their failure. This was due to loss of stability (buckling) of the compressed specimens before failure. This effect was obserdved from the first loading cycles. Therefore, tests with analogous loads for other structure densities were not performed so that the results would be a reference. The respective

values of applied load and number of cycles until failure of samples, with a specific degree of compaction of the diamond structure, are presented in Table 5. The selected hysteresis loops of samples subjected to fatigue tests are presented in figures 6-9, while the obtained fatigue life curves of Ti6Al4V titanium alloy with various degrees of diamond structure compaction (in double logarithmic scale) are presented in figure 10. It should be noted that the number of cycles until sample failure (fatigue life) strongly depends not only on the load amplitude but also on the degree of compaction of the diamond structure.

Table 5. Results of fatigue tests at individual load levels, obtained from monotonic tensile tests of samples of Ti6Al4V titanium alloy with diamond structure of different porosities [41]

				***p*=81%**				
σ_a^{eff} **[MPa]**	N_f	$\overline{N_f}$	σ_a^{eff} **[MPa]**	N_f	$\overline{N_f}$	σ_a^{eff} **[MPa]**	N_f	$\overline{N_f}$
12.5	63280	72162	**18.8**	16765	18079	**25.0**	6130	4773
	81665			19050			3035	
	71542			18423			5155	
31.3	1080	1150	**37.6**	585	427	**43.8**	188	188
	1230			295				
	1140			400				
				p=73%				
23.5	121440	116008	**35.2**	20015	24147	**46.9**	5185	7517
	114545			28390			9235	
	112040			24036			8130	
58.6	1980	2023	**70.3**	875	853	**84.7**	289	289
	2000			815				
	2090			868				
				p=50%				
48.8	173000	173152	**73.3**	29320	32817	**97.7**	9695	9062
	177095			35260			8350	
	169360			33872			9140	
122.1	3225	3227	**146.5**	1305	1328	**171.5**		370
	3245			1440			370	
	3210			1240				
				p=34%				
82.1	165750	150541	**123.2**	27230	26853	**164.2**	7720	7886
	113230			24665			7940	
	172643			28664			7998	
205.3	3005	2988	**246.3**	1224	1171	**287**		335
	3060			1270			335	
	2900			1020				

p=0%								
	300123			64096			32587	
293.3	331300	329974	**391.0**	86021	73353	**488.8**	38617	34226
	358500			69942			31476	
	12887			5612			1534	
586.6	10118	11529	**684.3**	5474	5528	**780.1**	1391	1471
	11583			5498			1488	

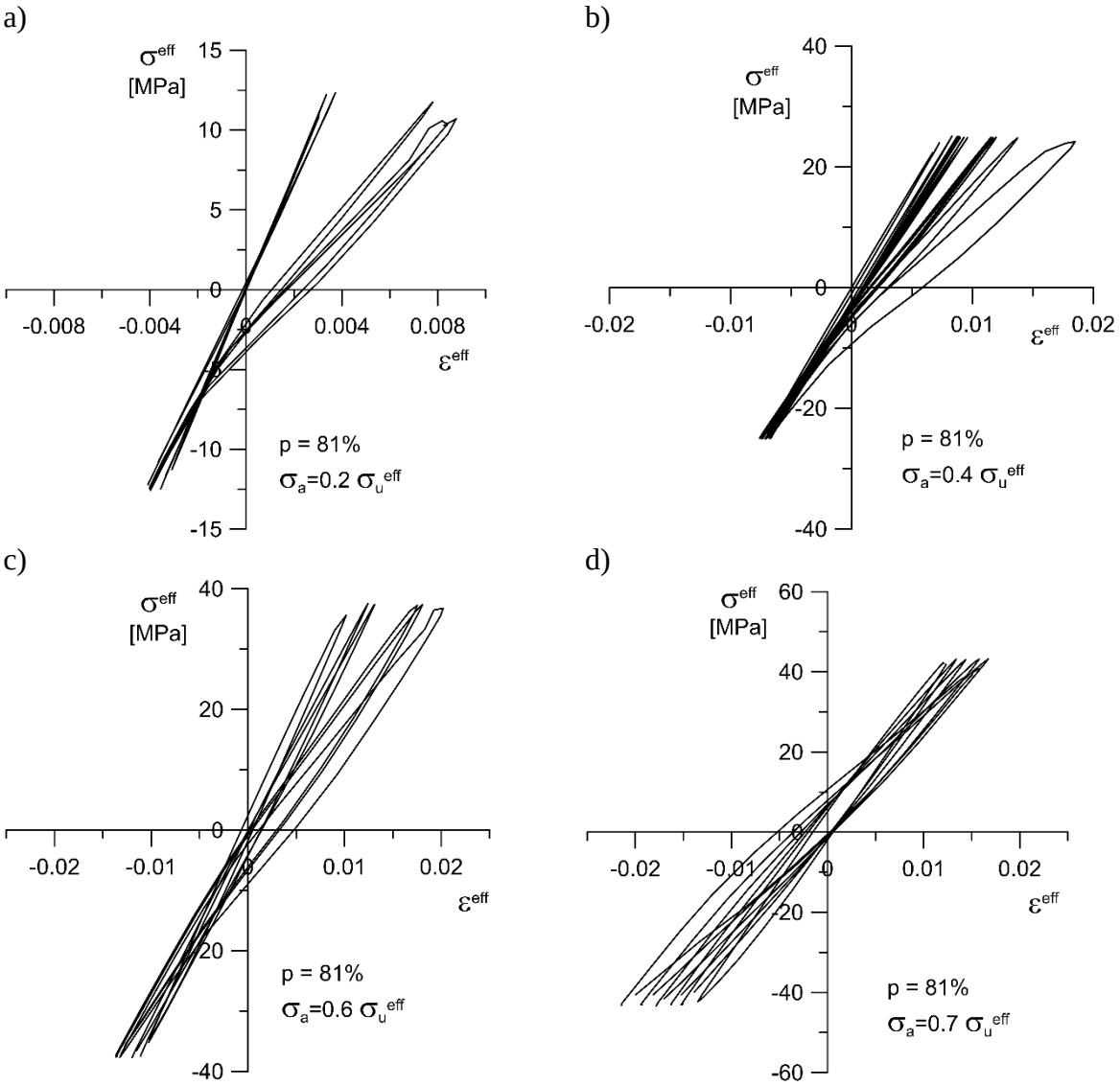

Fig. 6. Hysteresis loops of samples subjected to fatigue tests with diamond structure made of Ti6Al4V titanium alloy obtained by the LPBF method, with porosity *p*=81% and load amplitude at the level of: a) 0.2 σ_u^{eff}; b) 0.4 σ_u^{eff}; c) 0.6 σ_u^{eff}; d) 0.7 σ_u^{eff}

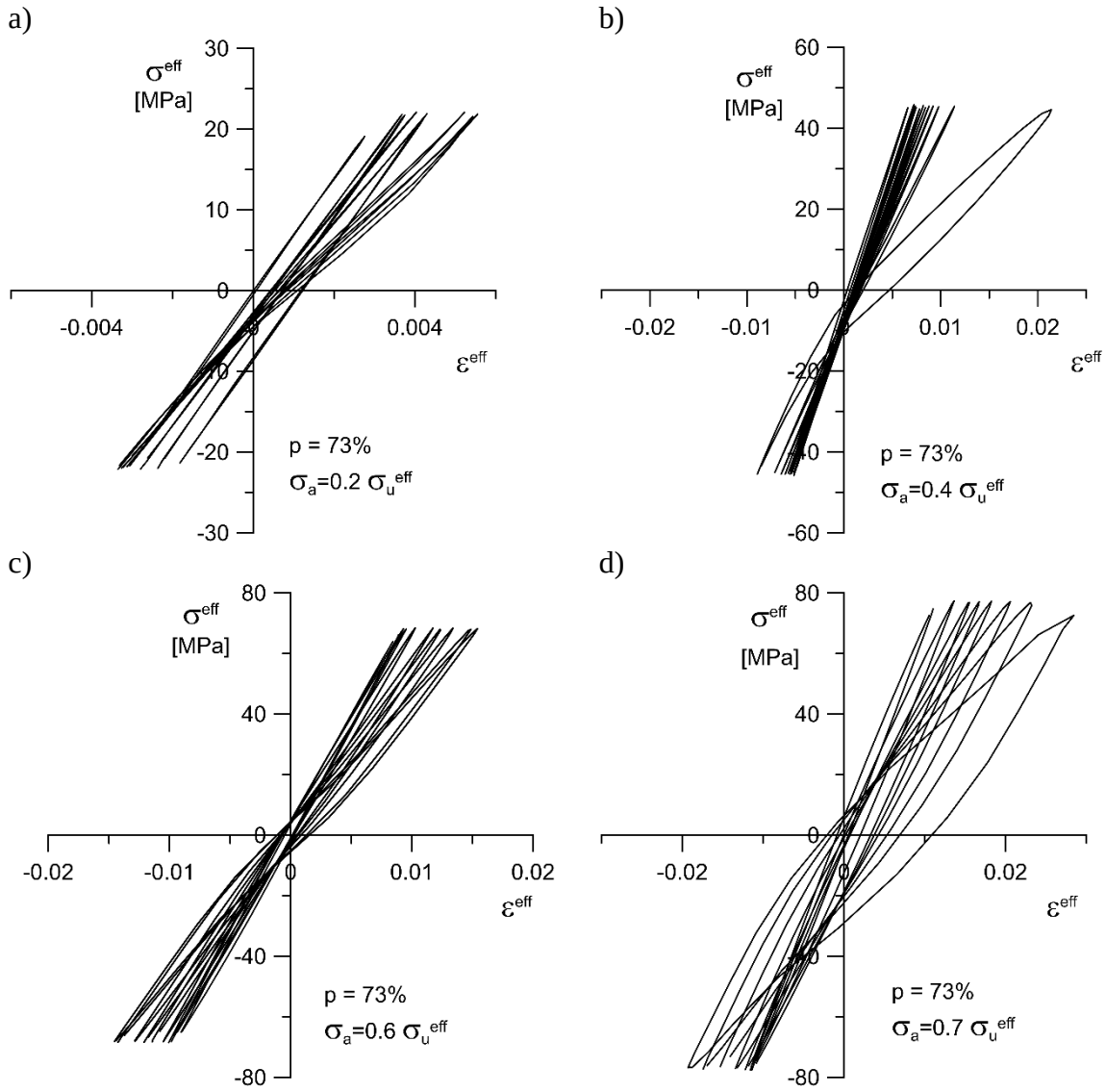

Fig. 7. Hysteresis loops of samples subjected to fatigue tests with diamond structure made of Ti6Al4V titanium alloy obtained by the LPBF method, with porosity p=73% and load amplitude at the level of: a) 0.2 σ_u^{eff}; b) 0.4 σ_u^{eff}; c) 0.6 σ_u^{eff}; d) 0.7 σ_u^{eff}

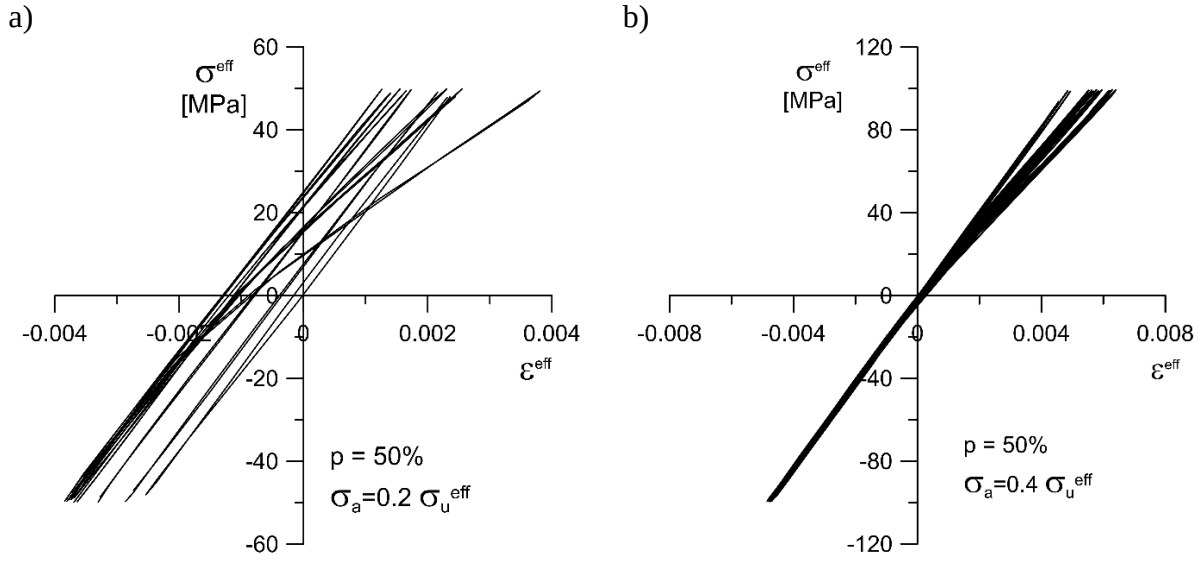

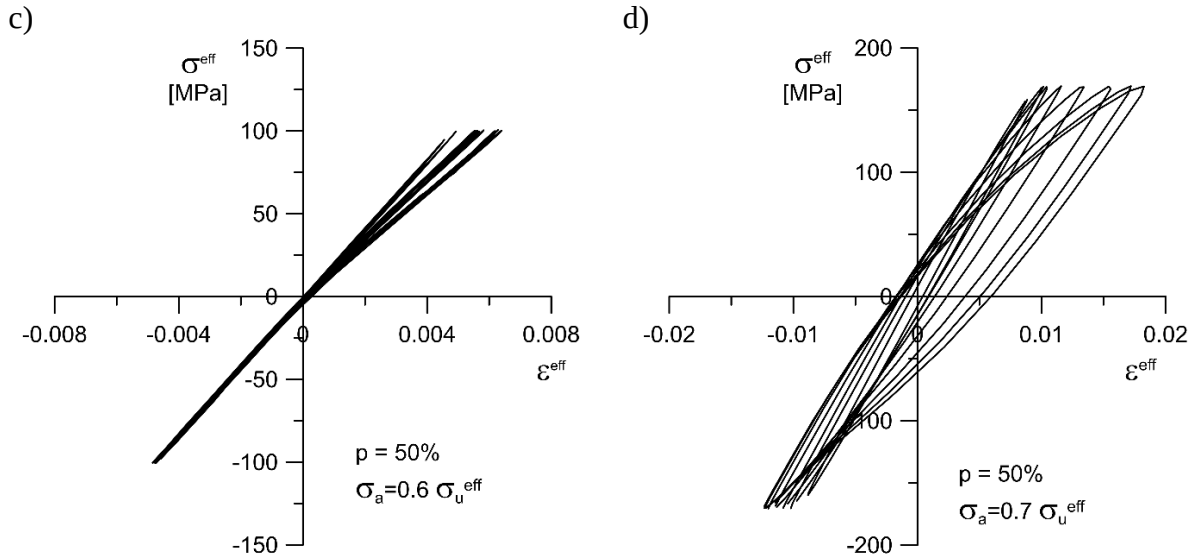

Fig. 8. Hysteresis loops of samples subjected to fatigue tests with diamond structure made of Ti6Al4V titanium alloy obtained by the LPBF method, with porosity p=50% and load amplitude at the level of: a) 0.2 σ_u^{eff} b) 0.4 σ_u^{eff}; c) 0.6 σ_u^{eff}; 0.7 σ_u^{eff}

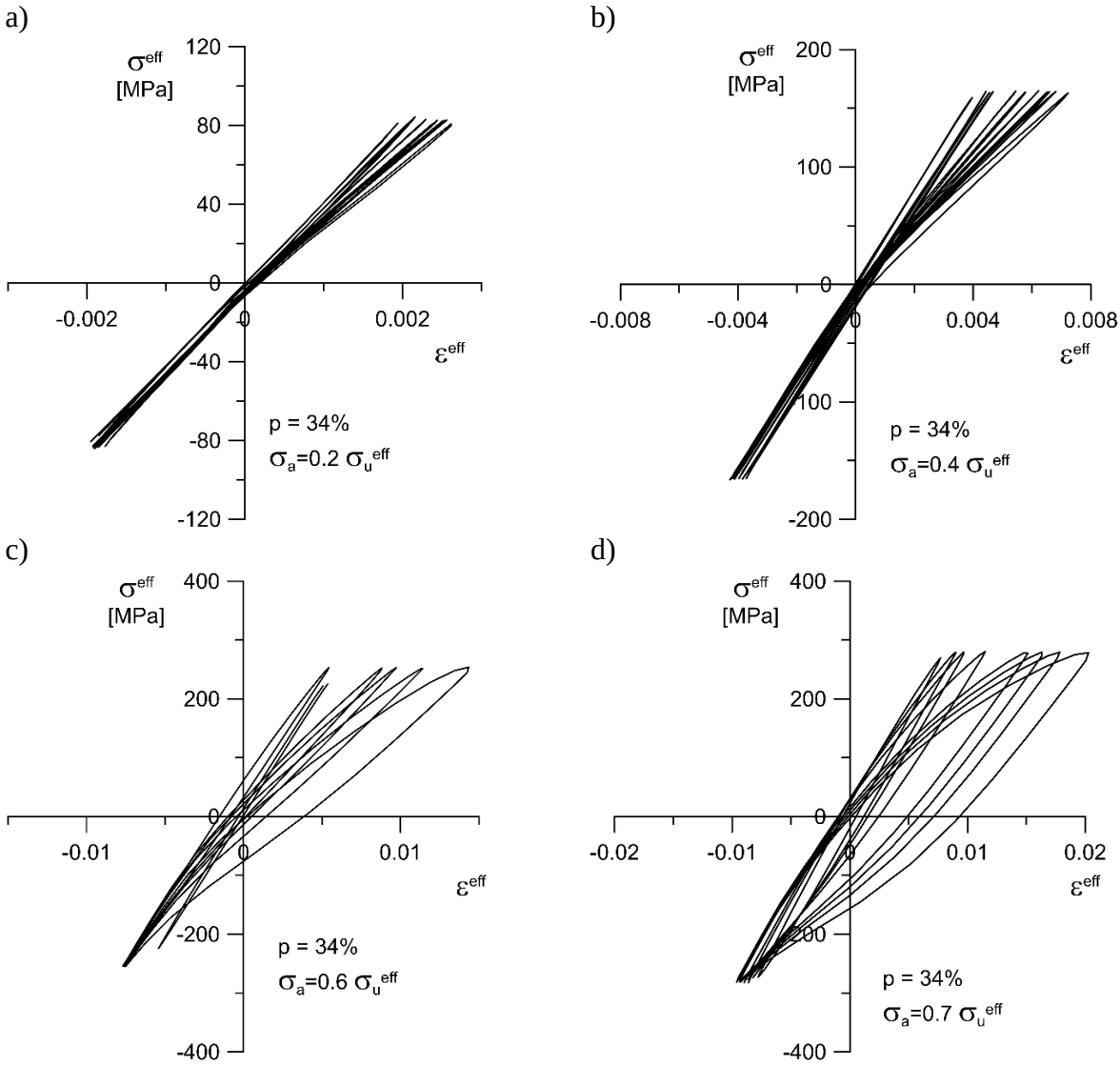

Fig. 9. Hysteresis loops of samples subjected to fatigue tests with diamond structure made of Ti6Al4V titanium alloy obtained by the LPBF method, with porosity p=34% and load amplitude at the level of: a) 0.2 σ_u^{eff}; b) 0.4 σ_u^{eff}; c) 0.6 σ_u^{eff}; d) 0.7 σ_u^{eff}

The course of the hysteresis loop for the tested samples is similar in all cases. Effective strain increases as the number of cycles increases. The exception are tests conducted at the amplitude level 0.2 σ_u^{eff} for samples with porosity of approx. 50% (fig. 8a). In this case, a negative increment of effective strain is observed in the first cycles, and in further fatigue cycles, this increment is positive. Deformation of the hysteresis loop can also be observed in the zone of tensile stress at the moment of fatigue crack initiation. This may be caused by the occurrence of microcracks in the fibers, which open in the "positive" range of fatigue loading (tension). In compression, the cracks are "closed", and the effect is not noticeable. However, in repeated loading cycles, the closed cracks probably do not open completely.

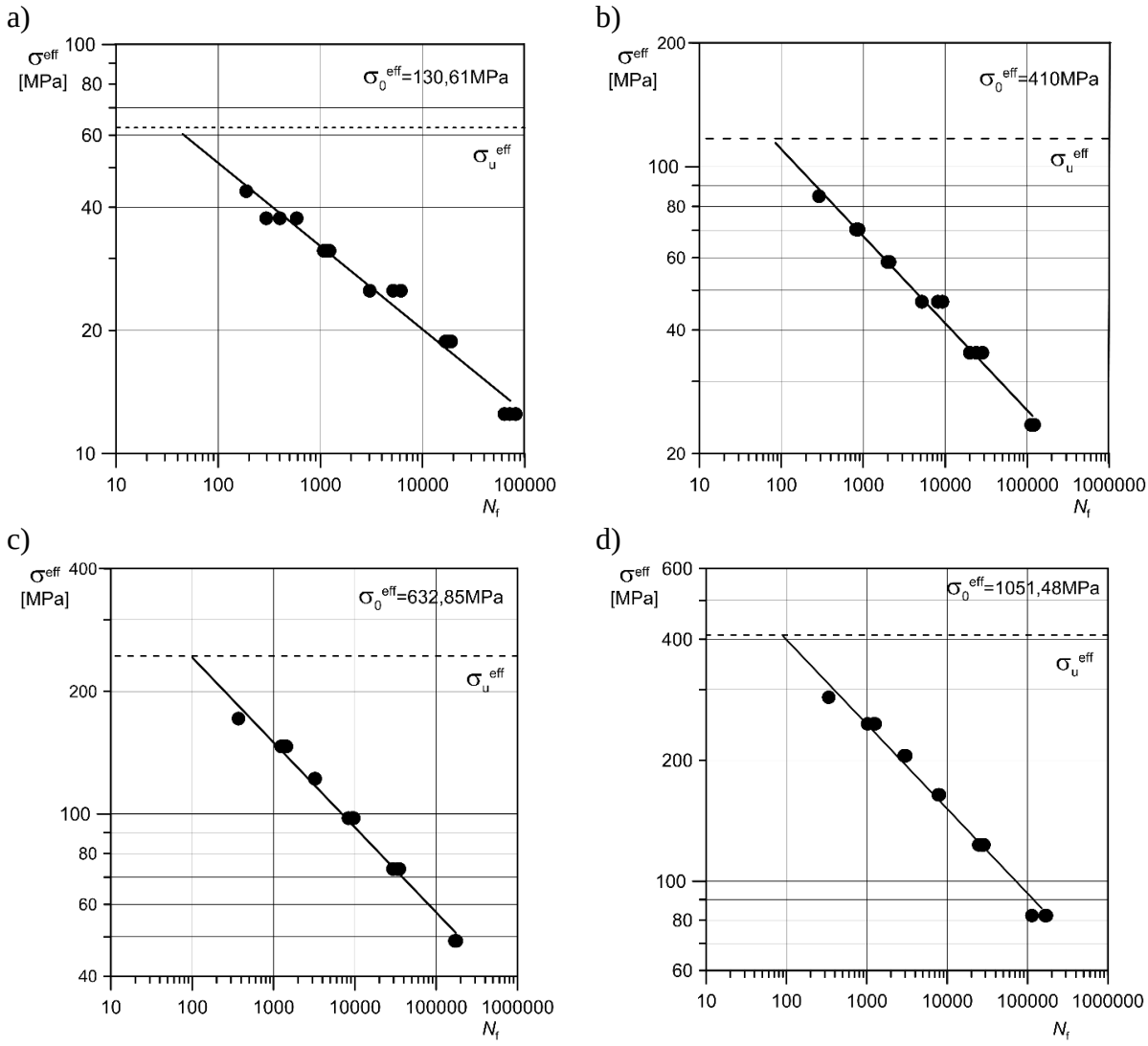

Fig. 10. Fatigue life curves of samples with diamond structures made of Ti6Al4V titanium alloy obtained by the LPBF method with porosities: a) p = 81%; b) p = 73%; c) p = 50%; d) p = 34%

Fatigue life curves of Ti6Al4V titanium alloys with diamond structures with different porosities obtained by the LPBF method were obtained by approximation of experimental data using a dependency in the following form:

$$\sigma_{\mathrm{a}}{}^{\mathrm{eff}} = \sigma_0{}^{\mathrm{eff}} N_{\mathrm{f}}{}^{\mathrm{c}}, \tag{1}$$

where:

$\sigma_{\mathrm{a}}{}^{\mathrm{eff}}$ - effective stress amplitude value, $\sigma_0{}^{\mathrm{eff}}$ – substitute value of effective tensile stress; c – exponent in this dependency, N_{f} – number of cycles until sample failure.

After taking the logarithm of dependency (1), can be obtained:

$$\log\sigma_{\mathrm{a}}{}^{\mathrm{eff}} = \log\sigma_0{}^{\mathrm{eff}} + c\log N_{\mathrm{f}}$$

or

$$\log\frac{\sigma_{\mathrm{a}}{}^{\mathrm{eff}}}{\sigma_0{}^{\mathrm{eff}}} = c\log N_{\mathrm{f}} \tag{2}$$

The values of coefficients present in dependencies (1) and (2) were determined on the basis of the experimental tests presented in figure 10, through approximation of experimental data in a logarithmic system with linear equations. Table 6 presents the results of calculations for various degrees of compaction of the diamond structure of Ti6Al4V titanium alloy. Only in the case of samples with near-zero porosity does the value of exponent c deviate from the rest. In other cases, the results are very similar. This also confirms the arrangement of fatigue life charts, which are nearly parallel for samples with non-zero porosity.

Table 6. Values of the coefficients present in dependency (1), determined on the basis of fatigue tests of Ti6Al4V titanium alloy with various degrees of diamond structure compaction

p [%]	$\sigma_{\mathrm{u}}{}^{\mathrm{eff}}$ [MPa]	$\sigma_0{}^{\mathrm{eff}}$	$\sigma_0{}^{\mathrm{eff}}/\sigma_{\mathrm{u}}{}^{\mathrm{eff}}$	c	R^2
81	62.6	130.61	2.086	-0.2030	0.9873
73	117.2	293.76	2.506	-0.2124	0.9925
50	244.2	632.85	2.591	-0.2085	0.9894
34	410.0	1051.48	2.565	-0.2104	0.9888
0	*975.1*	3277.9	*3.361*	-0.1873	0.9809

Effective tensile strength values of Ti6Al4V titanium alloy with various degrees of compaction of the diamond structure were referenced to the value of substitute effective tensile strength obtained through approximation of fatigue life curves according to formulas (1) and (2). It should be noted that the ratio of σ_0^{eff} to σ_u^{eff} is approx. 2.5 in nearly all cases. The exception is the structure with porosity p=81%. This may be due to the effect of the sample's low stiffness. In relation to this, under the influence of loads, the structure with porosity p=81% behaves more like a rod structure.

3. Numerical dependencies of the fatigue life of Ti6Al4V alloy with diamond structure

Figure 11 presents dependencies between normalized values of the effective stress amplitude and the number of cycles until sample failure. Stress was normalized by referencing the effective stress amplitude value to the effective tensile strength value (fig. 11a) and the value of substitute tensile strength (fig. 11b) of Ti6Al4V titanium alloys with various degrees of diamond structure compaction. It can be observed that the charts obtained in the logarithmic system are arranged nearly parallel to one another, while in figure 11b, they overlap, with the exception of the fatigue life curve for solid samples (with porosity near 0).

a)

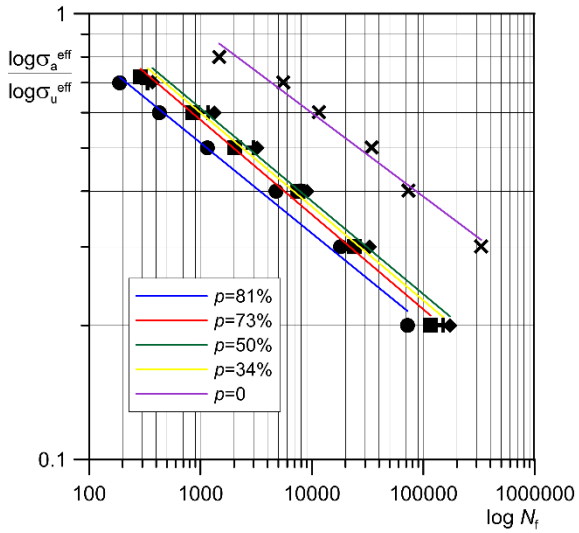

b)

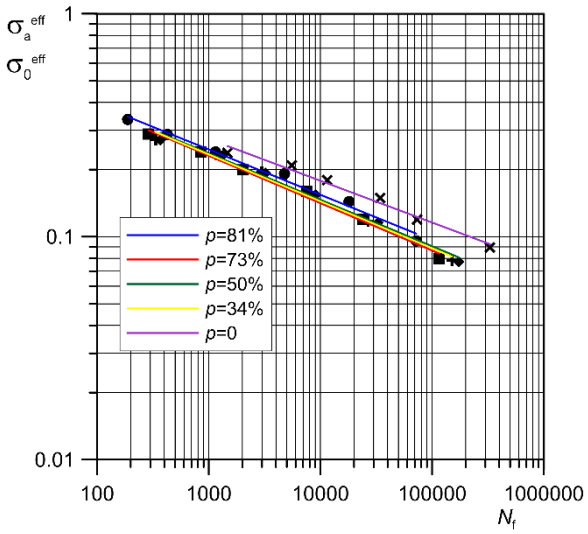

Fig. 11. Fatigue life curves normalized to average number of cycles until failure: a) ratio of effective stress amplitude value to effective tensile stress value; b) ratio of effective stress amplitude value to effective substitute tensile stress value

The numerical model of the fatigue life of Ti6Al4V titanium alloy with diamond structure was developed based on previously described results of experimental tests and the approach proposed in the paper by Falkowska and Seweryn [50], applied to forecast the fatigue life of samples made of 316L implant steel sinter with various porosities.

Normalized stress values are used in the model, i.e.:

$$\sigma^* = \frac{\sigma_a{}^{\mathrm{eff}}}{\sigma_0{}^{\mathrm{eff}}} \text{ and } \sigma^*_{\max} = \frac{\sigma_{\max}{}^{\mathrm{eff}}}{\sigma_0{}^{\mathrm{eff}}}, \tag{3}$$

where: $\sigma_a{}^{\mathrm{eff}}$ – effective stress loading the sample, $\sigma_{\max}{}^{\mathrm{eff}}$ – maximum effective stress in loading cycle, $\sigma_0{}^{\mathrm{eff}}$ – critical effective stress.

By introducing the effective scalar damage state variable ω, whose increment depends on the increment and value of effective stresses, namely:

$$\mathrm{d}\omega = n{\sigma^*}^{n-1}\mathrm{d}\sigma^* \qquad (\sigma^* > 0 \text{ i } \mathrm{d}\sigma^* > 0) \tag{4}$$

In one loading cycle (from 0 to $\sigma_{\max}{}^*$) the increment of the damage state variable is equal to:

$$\Delta\omega = \int_0^{\sigma^*_{max}} n{\sigma^*}^{n-1}\,\mathrm{d}\sigma^* = {\sigma^*_{max}}^n. \tag{5}$$

Assuming that fatigue crack initiation occurs when the variable reaches critical value, i.e.:

$$\omega = 1 \tag{6}$$

Accepting an identical increment $\Delta\omega$ in each loading cycle, can be obtained:

$$N_f \Delta\omega = N_f {\sigma^*_{max}}^n = 1, \tag{7}$$

after taking the logarithm, a dependency similar to (2) can be received, namely:

$$\log N_f + n\log\sigma^*_{max} = 0 \tag{8}$$

or

$$\log\sigma^* = -\frac{1}{n}\log N_f \tag{9}$$

Therefore, what remains is to determine the values of constants n and σ^* based on the results of experimental tests of the fatigue life of Ti6Al4V titanium alloy with diamond structure. Their values depend on the material's porosity (compaction). Comparing dependencies (1) and (8), the values of $n(p)$ can be obtained, which are given

in Table 7. It should be noted that the values of parameter n depend to a small extent on porosity, hence the averaged value can be accepted:

$$\bar{n} = \frac{1}{k}\sum_{i=1}^{k} n_i(p_i), \tag{10}$$

where n_i – parameter value for porosity p_i.

Table 7. Values of n constants based on the results of experimental tests of the fatigue life of Ti6Al4V titanium alloy with diamond structure.

p [%]	n	$\bar{n}$	R^2
81	4.92	4.793	0.9873
73	4.71		0.9925
50	4.79		0.9894
34	4.75		0.9888

The dependency between σ^* and number of cycles until failure N_f (9) for Ti6Al4V titanium alloy samples with diamond structure and different porosities, with an averaged value of the n parameter, is given in figure 12. It can be observed that, regardless of the degree of porosity, the dependencies obtained are arranged nearly linearly. Therefore, they can be approximated by a straight line with good accuracy. In this case, the lowest value of the coefficient of determination (R^2) is 0.9873, while the highest is 0.9925. It is also worth noting that the results obtained are in the area below the σ_u^{eff} value (dashed lines in Fig. 10).

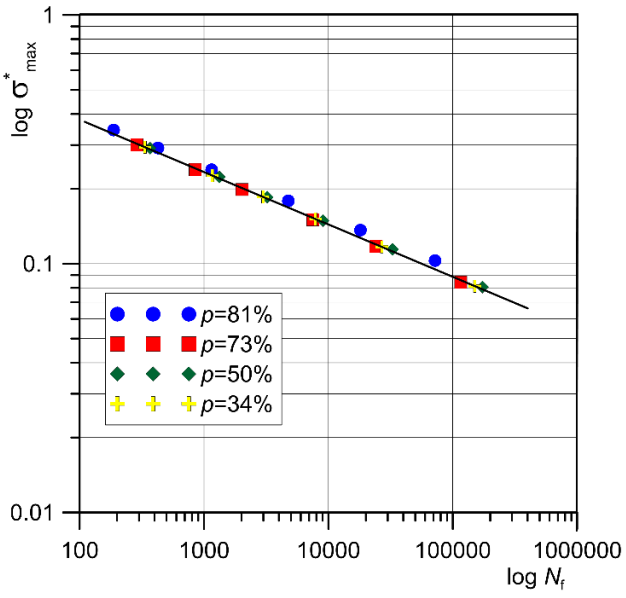

Fig. 12. Dependency between normalized, maximum effective stress in loading cycle and number of cycles until failure for Ti6Al4V titanium alloy samples with diamond structure and different porosities

4. Microscopic analysis of sample fractures

Observations of fatigue fractures of Ti6Al4V titanium alloy samples with diamond structure were conducted on a Phenom XL scanning electron microscope. Analyzing the resultant fractures, it can be stated that they differ depending on the degree of the structure's compaction as well as depending on the type of load applied during fatigue tests.

In the case of the structure with 81% porosity, cracks can be observed on the exterior surface of the scaffolding (fig. 13a) in the case of low-cycle tests. Cracking areas perpendicular to the direction of applied load are predominant on fatigue fracture surfaces (fig. 13b, 13e). Furthermore, particularly in the case of low-cycle tests, small cracks with a length up to 10 μm are visible (fig. 13c). The voids visible on fractures may indicate inter-particle cracking, the initiation of which took place in pores formed during building of the structure (fig. 13c, 13f).

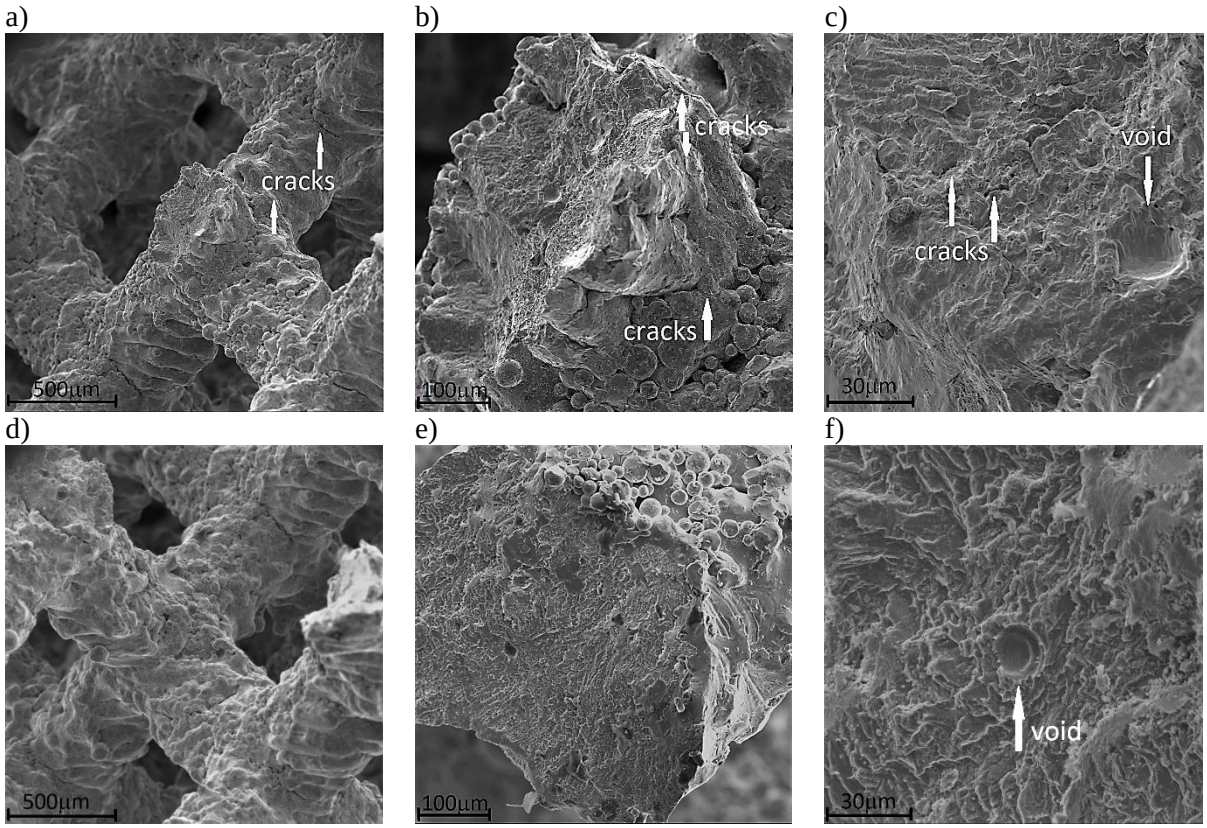

Fig. 13. Fatigue fractures of Ti6Al4V titanium alloy samples with 81% porosity, subjected to fatigue tests: low-cycle, with applied load amplitude $0.6\sigma_u^{eff}$ (a-c) and high-cycle, with applied load amplitude $0.2\sigma_u^{eff}$ (d-f)

In the case of analysis of the fatigue fractures of samples with 73% porosity subjected to low-cycle tests, it can be stated that they have a character similar to that of fractures in the case of 81% porosity. Cracks are

observed on the exterior of individual "struts" in the scaffolding (fig. 14a) as well as inside the structure (fig. 14b). The size of the cracks indicates that they formed on the grain boundaries of the powder from which samples were made. However, they are slightly larger than in the case of Ti6Al4V titanium alloy samples with the lowest degree of compaction in the structure.

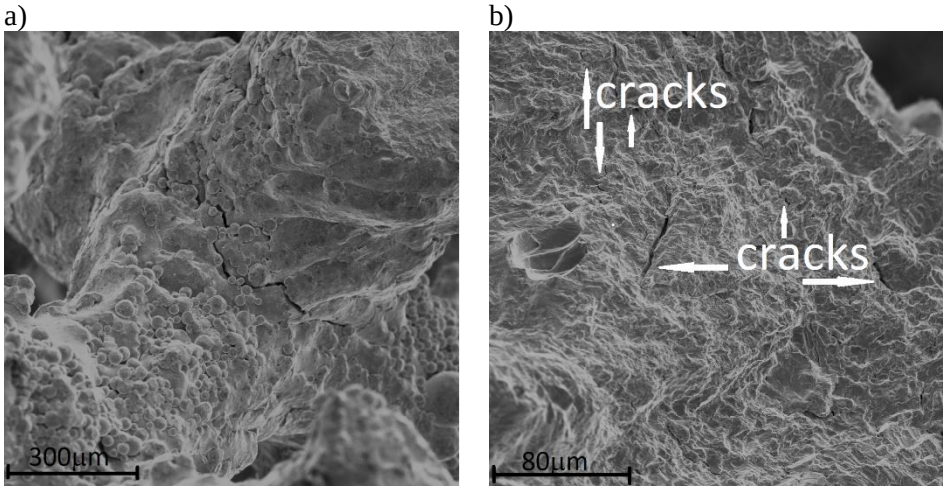

Fig. 14. Fatigue fractures of Ti6Al4V titanium alloy samples with 73% porosity, subjected to low-cycle fatigue tests, with applied load amplitude $0.6\sigma_u^{eff}$

Fractures of samples with 73% porosity subjected with fatigue tests with the application of a low stress amplitude have a slightly different character (fig. 15). Fractures primarily form at a certain angle consistent with the angle at which the porous structure was printed (fig. 15a). Large ductile fracture areas are observed (fig. 15b). One can also observe empty spaces formed as a result of detachment of individual grains (fig. 15a, 15b) as well as detachment of larger particles of material (fig. 15c). They suggest inter-particle cracking.

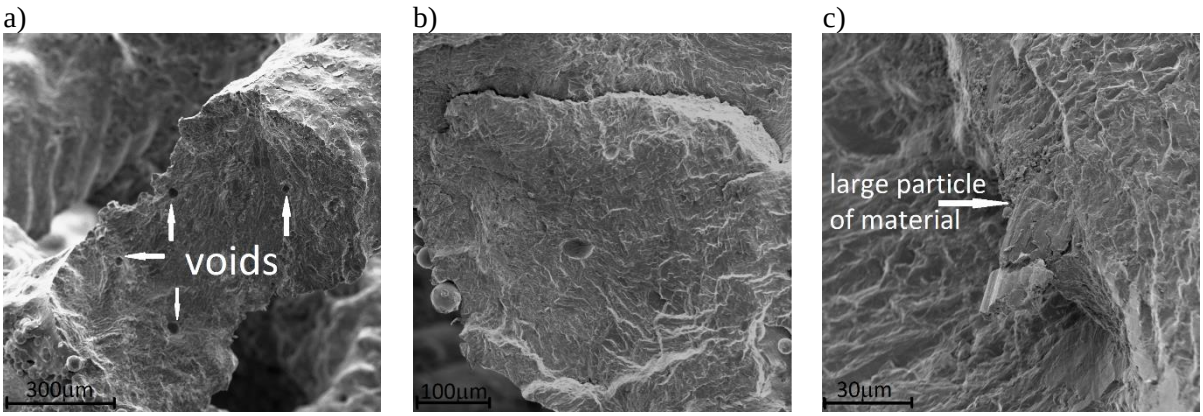

Fig. 15. Fatigue fractures of Ti6Al4V titanium alloy samples with 73% porosity, subjected to high-cycle fatigue tests, with applied load amplitude $0.2\sigma_u^{eff}$

In the case of observation of the fatigue fractures of samples with 50% porosity, lighter bands of ductile fracturing (fig. 16a) are observed, as well as areas where larger powder particles are detached. Fatigue bands with a regular, parallel arrangement, with a spacing of 3-4 μm can be observed on these bands (fig. 16b).

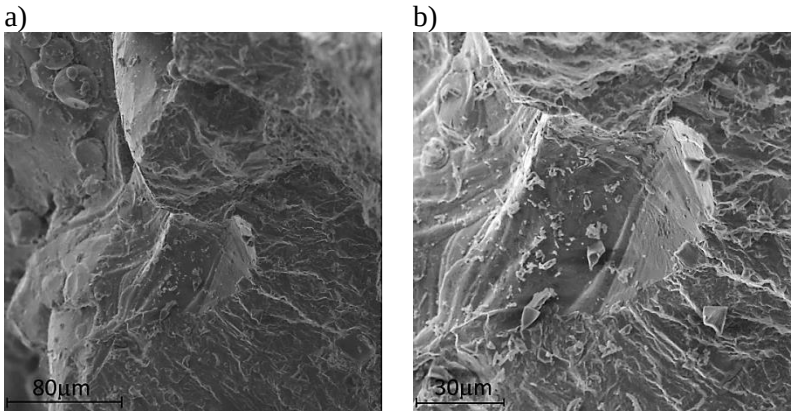

Fig. 16. Fatigue fractures of Ti6Al4V titanium alloy samples with 50% porosity, subjected to low-cycle fatigue tests with applied load amplitude $0.6\sigma_u^{eff}$

The surfaces of fatigue fractures in titanium alloy samples with 50% porosity, subjected to fatigue tests with the application of low stress amplitude values, are characterized by a larger number of cracks than in the previous cases. In addition, it can be observed that individual cracks have a length exceeding even 30 μm and a width of several μm (fig. 17b). Cyclic tension and compression of samples with a diamond structure produced using the LPBF method caused deformation of the fracture, on the surface of which numerous fatigue bands can be observed. They are arranged with a spacing of approx. 1 μm. It can only be observed at large magnifications (fig. 17c).

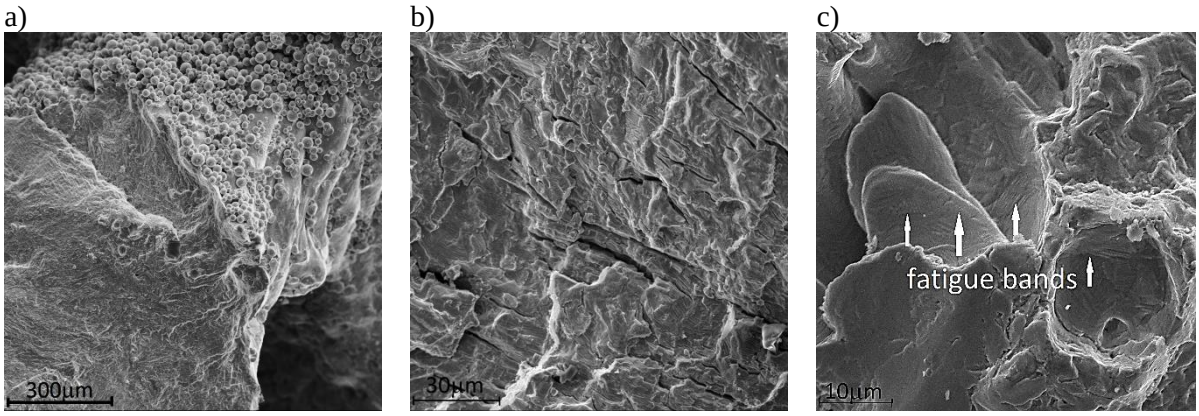

Fig. 17. Fatigue fractures of Ti6Al4V titanium alloy samples with 50% porosity, subjected to high-cycle fatigue tests with applied load amplitude $0.2\sigma_u^{eff}$

Fatigue fractures in samples of titanium alloy with diamond structure and 34% porosity, subjected to low-cycle fatigue tests, have a similar character to samples with 50% porosity (fig. 18). In truth, individual cracks occur on the surface of fractures, however their size is larger (fig. 18b). They can be the result of the splitting of larger powder particles.

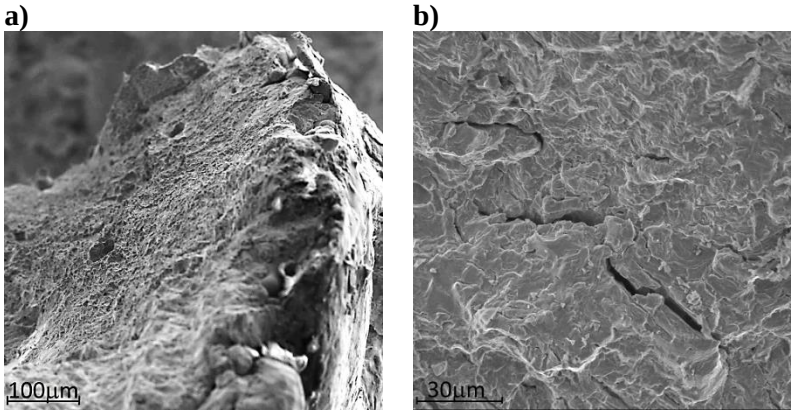

Rys. 18. Fatigue fractures of Ti6Al4V titanium alloy samples with 34% porosity, subjected to low-cycle fatigue tests with applied load amplitude $0.6\sigma_u^{eff}$

Observations of fatigue fractures of samples with 34% porosity, subjected to high-cycle tests, proved to be very interesting (fig. 19). The application of low stress amplitude values during fatigue tests results in the occurrence of areas of plastic deformations on their fractures (fig. 19c). Empty spaces are also observed (probably pores in the structure), with fatigue bands arranged in parallel to each other. This may indicate movement of the material's particles during cyclic tension and compression (fig. 19b). Cracks in the material can also be observed on fracture surfaces. However, they are more narrow (less plastically deformed) than in the case of structures tested with the application of a high stress amplitude (fig. 19d).

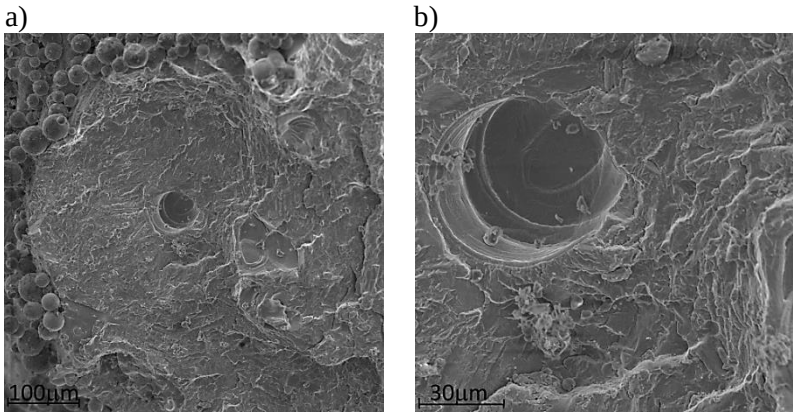

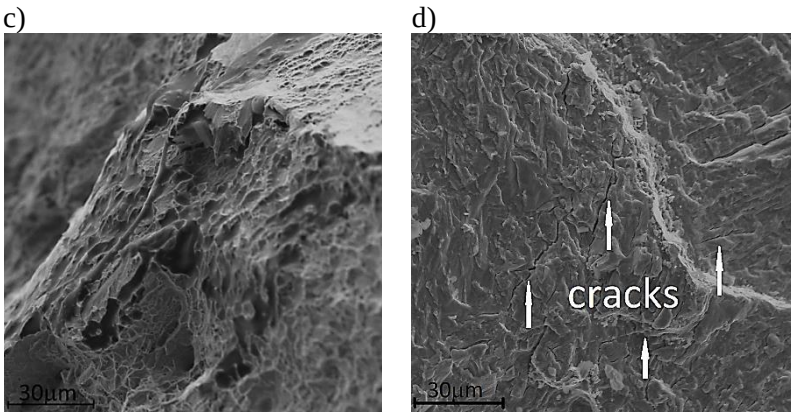

Fig. 19. Fatigue fractures of Ti6Al4V titanium alloy samples with 34% porosity, subjected to high-cycle fatigue tests with applied load amplitude $0.2\sigma_u^{eff}$

In the case of samples with a structure similar to that of solid material, a similar nature of fatigue fractures can be observed, regardless of the applied load amplitude (fig. 20a). Fractures are characterized by numerous cracks as well as by fatigue bands with various orientations (fig. 20b). This may arise from the arrangement of individual grains of powder during the Laser Power Bed Fusion process. In certain areas of the analyzed fractures, a fibrous structure typical of ductile fracture can be observed (fig. 20c).

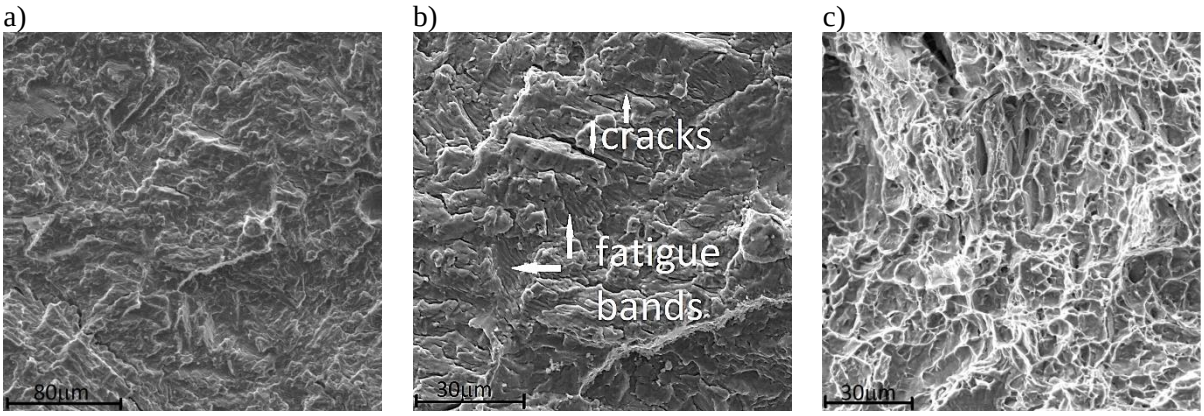

Fig. 20. Fatigue fractures of Ti6Al4V titanium alloy samples with a structure similar to that of solid material, subjected to fatigue tests with stress amplitude: $0.3\sigma_u^{eff}$ (a-b); $0.5\sigma_u^{eff}$ (c)

Conclusions

This paper presents the results of experimental fatigue life tests of samples with diamond structure and various porosities (34%, 50%, 73%, 81%) and made from solid material (with near-zero porosity), made of Ti6Al4V titanium alloy using the Laser Power Bed Fusion method. Tests showed a low number of fatigue loading cycles until initiation of the macro-crack in samples, even for low load levels, on the order of 20% tensile strength. This was caused by the presence of two types of notches:

- technological micro-notches between particles of melted powder, usually being the site of fatigue crack (inter-particle) initiation,
- notches related to the shape of the diamond structure itself.

Therefore, it is necessary to model stress and strain fields by means of the finite element method, with consideration of the actual structure of the material obtained by microtomography [49]. Then, it will be possible to determine the concentration of stresses and strains induced by both structural notches and technological micronotches and their influence on the metamaterial's fatigue life.

The effect of structural notches may be weakened by correcting the shape of the diamond structure produced by the Laser Power Bed Fusion method. This, of course, requires additional calculations using the finite element method, confirming reduction of stress and strain concentration, as well as experimental fatigue tests of the corrected structure, confirming an increase in fatigue life. A much more difficult problem, however, is to limit the influence of technological micro-notches, resulting directly from the nature of LPBF of titanium alloy particles. Powder particles have finite dimensions, and achieving a smooth surface would require additional processing that cannot be performed in the case of manufacturing a metamaterial with a diamond structure or similar to it.

The paper also proposes simple numerical dependencies of the fatigue life of the metamaterial with diamond structure with respect to its porosity and load values. To determine the number of loading cycles until crack initiation, it is necessary to determine only the tensile strength of the given metamaterial and the fatigue characteristic for the given porosity. These dependencies have a practical application, e.g. when designing components of joint endoprostheses using porous structures of metal alloys as substitutes for those made of solid material. This makes it possible to reduce the material's stiffness, which yields a positive effect that reduces the stress value in the zone of contact with bone. At the same time, however, a substantial drop in strength properties occurs, particularly in fatigue life, which this application severely limits.

Acknowledgements

This research was funded by the program of the Minister of Science and Higher Education (Poland) under the name "Regional Initiative of Excellence" in the years 2019–2022; project number 011/RID/2018/19, amount of financing 12000000 PLN

References:

[1] Roudnicka M, Mertova K, Vojtech D Influence of hot isostatic pressing on mechanical response of as-built SLM titanium alloy, IOP Conf. Series: Mater Sci Eng 2019;629:012034. https://doi:10.1088/1757-899X/629/1/012034.

[2] Gokuldoss PK, Kolla S, Eckert J Additive manufacturing processes: Selective laser melting, electron beam melting and binder jetting-selection guidelines, Materials 2017;10:672. https://doi.org/10.3390/ma10060672.

[3] Gu D, He B Finite element simulation and experimental investigation of residual stresses in selective laser melted Ti-Ni shape memory alloy, Comput Mater Sci 2016;117(6):221–232. https://doi.org/10.1016/j.commatsci.2016.01.044.

[4] Vrancken B, Thijs L, Kruth JP, Van Humbeeck J Heat treatment of Ti6Al4V produced by selective laser melting: microstructure and mechanical properties, J Alloy Compd 2012;541: 177–185. https://doi.org/10.1016/j.jallcom.2012.07.022.

[5] Wang D, Wang Y, Wu S, Lin H, Yang Y, Fan S, Gu C, Wang J, Song C Customized a Ti6Al4V bone plate for complex pelvic fracture by selective laser melting, Materials 2017;10(1):35. https://doi.org/10.3390/ma10010035.

[6] Deja M, Zieliński D, Kadir AZA, Humaira SN Applications of additively manufactured tools in abrasice machining – a literature review, Materials 2021;14:1318. https://doi.org/10.3390/ma14051318.

[7] Wycisk E, Emmelmann C, Siddique S, Walther F High cycle fatigue (HCF) performance of Ti-6Al-4V alloy processed by selective laser melting, Adv Mater Res 2013;816-817: 134-139. https://doi.org/10.4028/www.scientific.net/AMR.816-817.134.

[8] Li F, Li J, Huang T, Kou H, Zhou L Compression fatigue behavior and failure mechanism of porous titanium for biomedical applications, J Mech Behav Biomed Mater 2017;65:814-823. https://doi.org/10.1016/j.jmbbm.2016.09.035.

[9] Marin E, Fusi S, Pressacco M, Paussa L, Fedrizzi L Characterization of cellular solids in Ti6Al4V for orthopaedic implant applications: trabecular titanium, J Mech Behav Biomed Mater 2010;3:373-381. https://doi.org/10.1016/j.jmbbm.2010.02.001.

[10] Chen X, Wang D, Dou W, Wang Y, Yang Y, Wang J, Chen J Design and Manufacture of Bionic Porous Titanium Alloy Spinal Implant Based on Selective Laser Melting (SLM), Comp Model Eng Sci 2020;124(3):1099-1117. doi:10.32604/cmes.2020.09619.

[11] Amini M, Reisinger A, Pahr DH Influence of processing parameters on mechanical properties of a 3Dprinted trabecular bone microstructure, J Biomed Mater Res Part B; 20209108B):38–47. https://doi.org/10.1002/jbm.b.34363.

[12] Wong K, Scheinemann P Additive manufactured metallic implants for orthopaedic applications, Sci China Mater 2018;61(4):440-454. https://doi.org/10.1007/s40843-017-9243-9

[13] Liang C, Hu Y, Liu N, Zou X, Wang H, Zhang X, Fu Y, Hu J Laser Polishing of Ti6Al4V Fabricated by Selective Laser Melting, Metals 2020;10:191. https://doi.org/10.3390/met10020191.

[14] Grover T, Pandey A, Kumari ST, Awasthi A, Singh B, Dixit P, Singhal P, Saxena KK Role of titanium in bio implants and additive manufacturing: An overview, Materials Today: Proceedings 2020;26:3071-3080. https://doi.org/10.1016/j.matpr.2020.02.636.

[15] Tan XP, Tan YJ, Chow CSL, Tor SB, Yeong WY Metallic powder-bed based 3D printing of cellular scaffolds for orthopaedic implants: A state-of-the-art review on manufacturing, topological design, mechanical properties and biocompatibility, Mater Sci and Eng C 2017;(6):1328-1343. https://doi.org/10.1016/j.msec.2017.02.094.

[16] Chen Q, Thouas GA Metallic implant biomaterials, Mater Sci Eng R Rep 2015;87:1-57. https://doi.org/10.1016/j.mser.2014.10.001.

[17] Gepreel M, Niinomi M Biocompatibility of Ti-alloys for long-term implantation, J Mech Behav Biomed Mater 2013;20:407-415. https://doi.org/10.1016/j.jmbbm.2012.11.014.

[18] Caparrós C, Guillem-Marti J, Molmeneu M, Punset M, Calerom JA, Gil FJ Mechanical properties and in vitro biological response to porous titanium alloys prepared for use in intervertebral implants, J Mech Behav Biomed Mater 2014;39:79-86.

[19] Kumar A, Mandal S, Barui S, Vasireddi R, Gbureck U, Gelinsky M, Basu B Low temperature additive manufacturing of three dimensional scaffolds for bone-tissue engineering applications: Processing related challenges and property assessment, Mater Sci Eng R 2016;103:1-39. https://doi.org/10.1016/j.mser.2016.01.001.

[20] Murugan R, Ramakrishna S Development of Nanocomposites for Bone Grafting, Comp Sci Tech 2005;65:2385-2406. https://doi.org/10.1016/j.compscitech.2005.07.022.

[21] Wang X, Xu S, Zhou S, Xu W, Leary M, Choong P, Qian M, Brandt M, Xie YM Topological design and additive manufacturing of porous metals for bone scaffolds and orthopaedic implants: A review, Biomaterials 2016;83:127-141. https://doi.org/10.1016/j.biomaterials.2016.01.012.

[22] Taniguchi N, Fujibayashi S, Takemoto M, Sasaki K, Otsuki B, Nakamura T, Matsushita T, Kokubo T, Matsuda S Effect of pore size on bone ingrowth into porous titanium implants fabricated by additive manufacturing: An in vivo experiment, Mater Sci Eng C 2016;59:690-701. https://doi.org/10.1016/j.msec.2015.10.069.

[23] Chen SY, Huang JC, Pan CT, Lin CH, Yang TL, Huang YS, Ou CH, Chen LY, Lin DY, Lin HK, Li TH, Jang JSC, Yang CC, Microstructure and mechanical properties of open-cell porous Ti-6Al4V fabricated by selective laser melting, J All Comp 2017;713:248-254. https://doi.org/10.1016/j.jallcom.2017.04.190.

[24] Zhang S, Wei Q, Cheng L, Li S, Shi Y Effects of scan line spacing on pore characteristics and mechanical properties of porous Ti6Al4V implants fabricated by selective laser melting, Mater Des 2014;63:185-193. https://doi.org/10.1016/j.matdes.2014.05.021.

[25] Duan Y, Liu X, Zhang S, Wang L, Ding F, Song S, Chen X, Deng B, Song Y Selective laser melted titanium implants play a positive role in early osseointegration in type 2 diabetes mellitus rats, Dent Mater J 2020;39(2):214–221. https://doi.org/10.4012/dmj.2018-419

[26] Al-Tamimi AA, Hernandez MA, Omar A, Morales-Aldana DF, Peach C, Bartolo P Mechanical, biological and tribological behaviour of fixation plates 3D printed by electron beam and selective laser melting, Int J Adv Manuf Technol 2020;109:673–688. https://doi.org/10.1007/s00170-020-05676-1.

[27] Costa Santos E, Shiomi M, Osakada K, Laoui T Rapid manufacturing of metal components by laser forming, Int J Mach Tools Manuf 2006;46:1459–1468. https://doi.org/10.1016/j.ijmachtools.2005.09.005.

[28] Píška M, Trubačová P, Hornıíkova J, Deblir I Analysis of powder steel material, laser sintering technology and machining on surface parameters and fatigue, Mat Wer 2017;48(8):820–830. https://doi.org/10.1002/mawe.201700030.

[29] Ran Q, Yang W, Hu Y, Shen X, Yu Y, Xiang Y, Cai K Osteogenesis of 3D printed porous Ti6Al4V implants with different pore sizes, J Mech Behav Biomed Mater 2018;84:1-11. https://doi.org/10.1016/j.jmbbm.2018.04.010.

[30] Nyoni E, Akinlabi ET Process parameter interaction effect on the evolving properties of laser metal deposited titanium for biomedical applications, Thin Solid Films 2016;620:94-102. https://doi.org/10.1016/j.tsf.2016.09.060.

[31] Čapek J, Machová M, Fousová M, Kubásek J, Vojtěch D, Fojt J, Jablonská E, Lipov J, Ruml T Highly porous, low elastic modulus 316L stainless steel scaffold preparedby selective laser melting, Mater Sci Eng C 2016;69:631-639. https://doi.org/10.1016/j.msec.2016.07.027.

[32] CuadradoA, Yánez A, Martel O, Deviaene S, Monopoli D Influence of load orientation and of types of loads on the mechanical properties of porous Ti6Al4V biomaterials, Mater Des 2017;135:309-318. https://doi.org/10.1016/j.matdes.2017.09.045.

[33] Lipowiecki M, Ryvolova M, Tottosi A, Kolmer N, Naher S, Brennan SA, Vazquez M, Brabazon D Permeability of rapid prototyped artificial bone scaffold structures, Rapid Prototyped Artificial Bone Scaffold Structures, J Biomed Mater Res A 2014;102A:4127–4135.https://doi.org/10.4028/www.scientific.net%2FAMR.445.607.

[34] Choo H, Sham K, Bohling J, Ngo A, Xiao X, Ren Y, Depond PJ, Matthews MJ, Garlea E Effect of laser power on defect, texture, and microstructure of a laser powder bed fusion processed 316L stainless steel, Mater Des 2019;164:107534. https://doi.org/10.1016/j.matdes.2018.12.006.

[35] du Plessis A Effects of process parameters on porosity in laser powder bed fusion revealed by X-ray tomography, Add Manuf 2019;30:100871. https://doi.org/10.1016/j.addma.2019.100871.

[36] Sterling AJ, Torries B, Shamsaei N, Thompson SM, Seely DW Fatigue behavior and failure mechanisms of direct laser deposited Ti–6Al–4V, Mater Sci Eng A 2016;655:100-112. https://doi.org/10.1016/j.dib.2016.01.059.

[37] Günther J, Krewerth D, Lippmann T, Leuders S, Tröster T, Weidner A, Biermann H, Niendorf T Fatigue life of additively manufactured Ti–6Al–4V in the very high cycle fatigue regime, Int J Fatigue 2017;94:236-245. https://doi.org/10.1016/j.ijfatigue.2016.05.018.

[38] McGregor M, Patel S, McLachlin S, Vlasea M Data related to architectural bone parameters and the relationship to Ti lattice design for power bed fusion additive manufacturing Add Manuf 2021; 47: 102273. https://doi.org/10.1016/j.dib.2021.107633

[39] Karolewska K, Ligaj B, Wirwicki M, Szala G Strength analysis of Ti6Al4V titanium alloy produced by the use of additive manufacturing method under static load conditions, J Mater Research Technol 2020;9(2):1365-1379. https://doi.org/10.1016/j.jmrt.2019.11.063.

[40] Wu M-W, Chen J-K, Lin B-H, Chiang P-H Improved fatigue endurance ratio of additive manufactured Ti-6Al-4V lattice by hot istostatic pressing, Mater Des 2017;143:163-170. http://dx.doi.org/10.1016/j.matdes.2017.08.048

[41] Falkowska A, Seweryn A, Skrodzki M, Strength properties of a porous titanium alloy Ti6Al4V with diamond structure obtained by Laser Power Bed Fusion (LPBF), Materials 2020;13(22):5138. https://doi.org/10.3390/ma13225138.

[42] Sausto F, Marchese G, Bassini E, Calandri M, Biamino S, Ugues D, Foletti S, Beretta S, Anisotropic mechanical and fatigue behaviour of Inconel718 produced by SLM in LCF and high-temperature conditions, Fatigue Fract Eng Mater Struct, 2021;44:271–292. https://onlinelibrary.wiley.com/doi/epdf/10.1111/ffe.13373.

[43] Soro N, Saintier N, Merzeau J, Veidt M, Dargusch MS Quasi-static and fatigue properties of graded Ti-6Al-4V lattices produced by Laser Power Bed Fusion (LPBF) Add Manuf 2021;37:101653. https://doi.org/10.1016/j.addma.2020.101653

[44] Yavari A, Ahmadi SM, Wauthle R, Pouran B, Schrooten J, Weinans H, Zadpoor AA Relationship between unit cell type and porosity and the fatigue behavior of selective laser melted meta-biomaterials J Mech Behav Biomed Mater 2015; 43:91-100. https://doi.org/10.1016/j.jmbbm.2014.12.015

[45] Van Hooreweder B, Kruth J, Advanced fatigue analysis of metal lattice structures produced by Selective Laser Melting, CIRP Annals - Manuf Tech 2017;66:221-224. https://doi.org/10.1016/j.cirp.2017.04.130.

[46] Metal Additive Manufacturing with the ProX™ DMP 3D printers http://3dsystemspolska.pl/files/download/3dsystemspolska_dmp_specyfikacja_201602_web.pdf, (last access 28.12.2021)

[47] Dallago M, Fontanari V, Winiarski B, Zanini F, Carmignato S, Benedetti M, Fatigue properties of Ti6Al4V cellular specimens fabricated via SLM: CAD vs real geometry, Proc Struct Int 2017;7:116-123. https://doi.org/10.1016/j.prostr.2018.12.027.

[48] Dallago M, Winiarski B, Zanini F, Carmignato S, Benedetti M, On the effect of geometrical imperfections and defects on the fatigue strength of cellular lattice structures additively manufactured via Selective Laser Melting, Int J Fatigue 2019;124:348-360. https://doi.org/10.1016/j.ijfatigue.2019.03.019.

[49] Doroszko M, Falkowska A, Seweryn A Image-based numerical modeling of the tensile deformation behavior and mechanical properties of additive manufactured Ti–6Al–4V diamond lattice structures, Mater Sci Eng A 2021;818:1-17. https://doi.org/10.1016/j.msea.2021.141362.

[50] Falkowska A, Seweryn A Fatigue life of 316L steel sinters of varying porosity under conditions of uniaxial periodically variable loading at a fixed stress amplitude, Int J Fatigue 2018;117:496-510. https://doi.org/10.1016/j.ijfatigue.2018.07.025.